ARTICLE

Laser-Induced Frequency Tuning of Fourier-Limited Single-Molecule Emitters

Maja Colautti, Francesco S. Piccioli, Zoran Ristanović, Pietro Lombardi, Amin Moradi, Subhasis Adhikari, Irena Deperasinska, Boleslaw Kozankiewicz, Michel Orrit,* and Costanza Toninelli*

Read Online

ACCESS | Metrics & More | Article Recommendations | SI Supporting Information

ABSTRACT: The local interaction of charges and light in organic solids is the basis of distinct and fundamental effects. We here observe, at the single-molecule scale, how a focused laser beam can locally shift by hundreds of times their natural line width and, in a persistent way, the transition frequency of organic chromophores cooled at liquid helium temperature in different host matrices. Supported by quantum chemistry calculations, the results can be interpreted as effects of a photoionization cascade, leading to a stable electric field, which Stark-shifts the molecular electronic levels. The experimental observation is then applied to a common challenge in quantum photonics, *i.e.*, the independent tuning and synchronization of close-by quantum emitters, which is desirable for multiphoton experiments. Five molecules that are spatially separated by about 50 μm and originally 20 GHz apart are brought into resonance within twice their line width. This tuning method, which does not require additional fabrication steps, is here independently applied to multiple emitters, with an emission line width that is only limited by the spontaneous decay and an inhomogeneous broadening limited to 1 nm. The system hence shows promise for photonic quantum technologies.

KEYWORDS: single molecule, optical tuning, organic semiconductors, single-photon sources, Stark shift
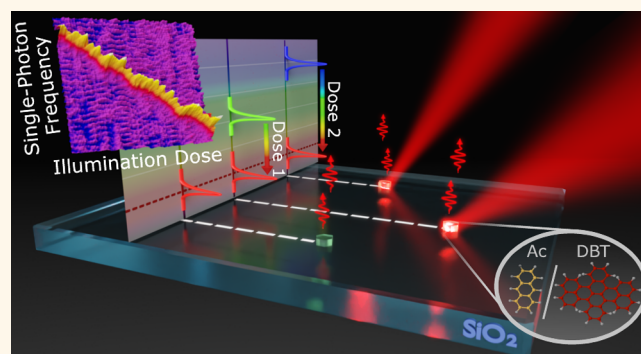
Single fluorescent molecules of polycyclic aromatic hydrocarbons (PAHs) embedded in crystalline organic matrices are widely considered highly coherent, stable, and bright two-level quantum systems in the solid state.[1−5] Indeed, they can be operated as single-photon sources,[6] combining high count rate and Fourier-limited line widths,[7−9] or as nanoprobes with exquisite sensitivity to electric fields, pressure, and strain.[10,11] PAH-based quantum devices can also be readily integrated in photonic chips.[12−15] A major advantage of PAH systems resides in the possibility to mass produce nominally identical fluorescent molecules at low costs and still obtain outstanding optical and optoelectronic properties. PAHs are under investigation for their use also in organic solar cells,[16] as well as in super-resolution microscopy methods.[17] Furthermore, the Stark effect is a well-established technique for tuning the molecular transitions.[18−20] Broad tunability has been demonstrated for instance in the case of anthracene nanocrystals (Ac NCXs) doped with dibenzoterrylene (DBT) molecules, exhibiting a quadratic Stark shift upon the application of a voltage bias (tuning range >400 GHz, comparable to the inhomogeneous broadening).[21] Also a large linear and homogeneous Stark shift has been achieved, embedding DBT in 2,3-dibromonaphthalene (DBN), suggest-

ing the system as a promising nanoprobe of electric fields and charges.[22]

Such previous results demonstrate the potential of molecular-based techniques which, in principle, could also go beyond single-emitter devices. However, current tuning methods have to be scaled up, allowing for local control of the transition frequency. This is crucial to optimize coupling of multiple emitters to photonic structures, as well as quantum interference among distinct sources on chip. To this purpose, electrical tuning of the emission wavelength for multiple sources is challenging to implement. Optical control might instead enable simple, fast, and independent frequency tuning of separated emitters. Recent promising works have shown laser-induced frequency tuning of epitaxial quantum dots' transitions. Physical manipulation of the sample is in this case
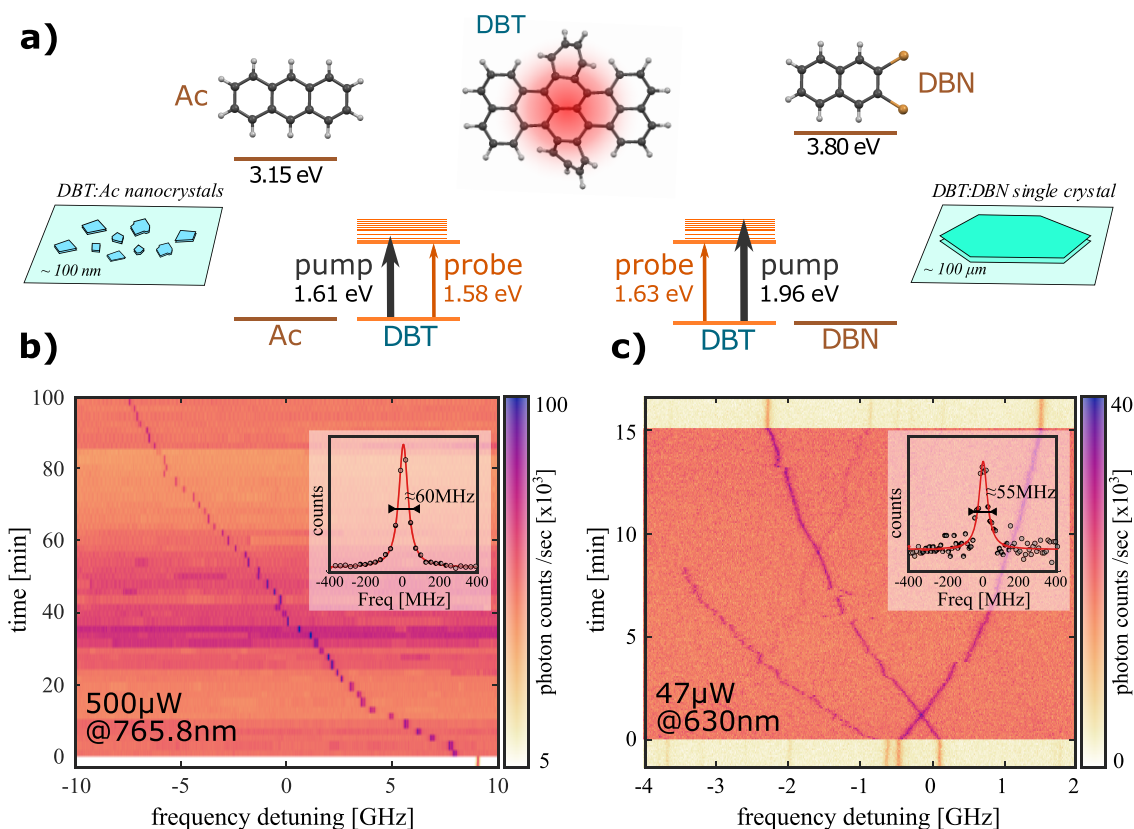
Figure 1. (a) Chemical structures of the guest (DBT) and host molecules (Ac, DBN) used in this study. The energies of the pump and probe beams used in the experiments are indicated for comparison. (b, c) Laser-induced frequency shift for DBT in Ac (b) and DBT in DBN (c). The fluorescence count rate is plotted in color scale as a function of the excitation laser frequency, scanning over the molecular ZPL. The measurements are repeated in time, while the pump laser is switched on. The pump presence is recognized by the onset of a strong background signal; that is, the light yellow background represents scans without the pump beam. Insets in panels (b) and (c) represent horizontal cuts and include the Lorentzian fits to the data.

confined within the laser beam diameter, and localized tuning of the emitters is achieved *via* thermal annealing,[23] mechanical expansion through phase-change materials,[24] or controlled strain through the host/substrate medium.[25] Nevertheless, the observed decoherence and spectral diffusion of the emitters' line width can be detrimental in many applications.

In this work we demonstrate fabrication-free, micron-resolved, optical frequency tuning of individual DBT molecules. We attribute the laser-induced frequency tuning of the molecular zero-phonon line (ZPL) to a local Stark shift, associated with optically induced long-lived charge-separated states, which notably persists for at least several hours after the pump laser is switched off. We first demonstrate the versatility of the concept, studying DBT in two different types of molecular crystals. A full characterization of the laser-induced frequency tuning is presented. In particular, we show how the magnitude of the induced spectral shift can be extended over a broad frequency range, by acting on the pump laser parameters. We also verify that close-to-Fourier-limited emission and photostability are preserved at cryogenic temperatures after the tuning process. In the following section, we demonstrate the scalability of the presented method as we show independent tuning of individual emitters down to 15 μm in proximity. In particular, we prove that the method can be extended to the frequency scale of the inhomogeneous line broadening, achieving spectral shifts that are more than 3 orders of magnitude larger than the natural line width. We show ZPL frequency matching (within two line widths) of five

molecular emitters, all within a 50×50 μm area and initially >20 GHz apart in frequency. Finally, we propose a model based on the photoionization mechanism of charge generation and support it with low-level quantum chemistry calculations. Different routes for the charge generation process, which may be an alternative or concurrent to the one described by our model, are also briefly discussed.

Overall, the possibility of using an all-optical approach to shift the transition frequency of individual emitters while maintaining coherent spectral properties offers a promising tool for applications in quantum nanophotonics. In particular, the presented results will benefit the realization of scalable quantum photonic devices and protocols based on multiple photons and multiple single-molecule emitters. More generally, the concept of laser-induced charge separation *via* photoionization of molecules can have broader scope in applications of single-molecule emitters, for example in nanoscale sensing of charge-carrier generation and in understanding the photoconductivity and photorefraction of organic semiconductors.

RESULTS AND DISCUSSION

Laser-Induced Tuning of Single-Molecule Emission. The optically induced frequency tuning of light emission is studied *via* single-molecule measurements on DBT chromophores embedded in two different host systems, namely, anthracene (Ac) nanocrystals doped with low DBT concentration ($\sim 10^{-2}$ molecules/GHz) and DBN crystal flakes,
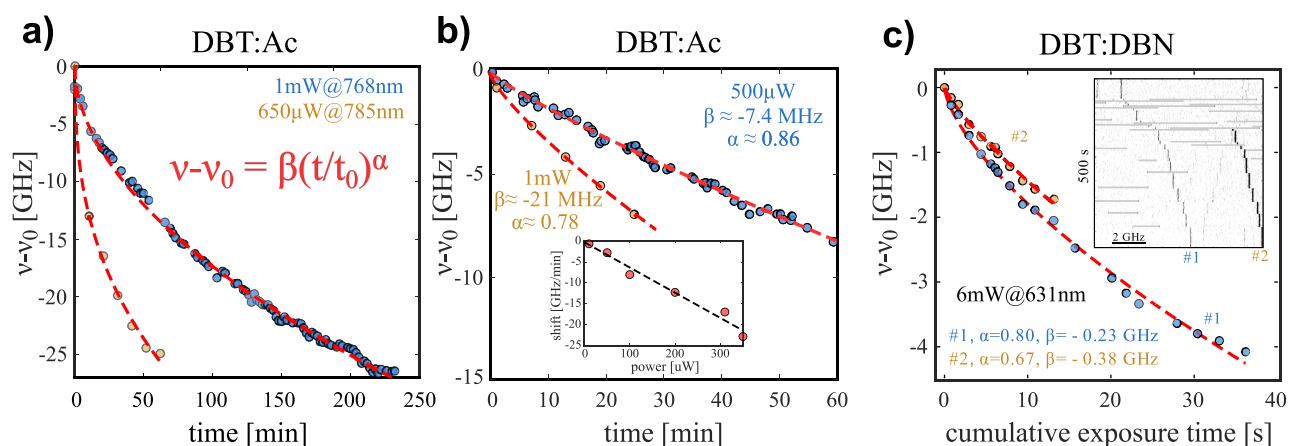
Figure 2. Dependence of the laser-induced shift on the exposure time and pump power for DBT:Ac (a, b) and DBT:DBN (c). The data points are the ZPL resonant frequencies obtained from a Lorentzian fit to the real-time excitation spectra, while the red dashed lines are power-law fits to the data. (a) Spectral shifts for pump laser frequency around the 0−1 transition (blue points) and tuned 10 GHz below ν_0 (yellow points) are compared. (b) Spectral shift dynamics for a DBT emitter pumped with different laser power. Inset: Spectral shifts of a second molecule subject to several 2 min long bursts at increasing power show a linear dependence on pump beam power. (c) Spectral shift as a function of cumulative exposure time for two DBT emitters (indicated as #1 and #2) in DBN. Inset: Frequency scans shown in real time (one line scan is 5 s). The gray horizontal lines indicate intermittent, short pump laser exposures (0.5 to 3 s).

doped with high DBT concentration (∼1 molecule/GHz). The molecular components of the two studied systems and their electronic energy levels are summarized in Figure 1a. We also report additional results on a third system of DBT in naphthalene in the SI, showing that the effect applies to a broader range of organic crystals. The studied systems share the same guest molecule (DBT), but are known to have different response to the electric field. In particular, DBT:DBN exhibits a large linear Stark coefficient due to the broken inversion symmetry of guest DBT molecules,[22] while DBT:Ac shows a quadratic Stark coefficient.[7,21]

All the experiments are performed at liquid helium temperatures. In these conditions, the purely electronic ZPL is about 40 to 60 MHz wide. The spectral line shape can be traced with a standard epifluorescence microscope by scanning the frequency of the CW excitation laser (named "probe" hereafter) around the resonant wavelength. The Stokes-shifted fluorescence, spectrally selected through a long-pass filter, is correspondingly measured with an avalanche photodiode, giving access to the excited state occupation probability as a function of the excitation wavelength.

Optical frequency tuning of the narrow-band ZPL is achieved by focusing on the target crystalline regions a second CW laser (named "pump" hereafter), generally operating at a different wavelength and higher intensity. In Figure 1b,c, real-time information on the laser-induced shift is provided by color maps showing, as a function of time, the excitation spectra of DBT molecules, exposed to the pump laser for a long time interval. In Figure 1a, simplified Jablonski diagrams are outlined, showing as well the energies of the pump and probe lasers employed in the experiments. The probe laser is scanned over the ZPL transitions around 785 nm for DBT:Ac (Figure 1b) and 756 nm for DBT:DBN (Figure 1c), whereas the pump laser is centered at 765.8 and 630 nm, respectively.

Zero-phonon lines corresponding to different molecules can thus be initially identified, followed during the burst duration above the background fluorescence, and recovered at different frequency positions after the exposure (Figure 1c). It is worth noticing that after the pump laser illumination DBT molecules preserve excellent spectral stability and close-to-lifetime limited

resonance line width. In particular, the spectral width amounts to ∼60 and ∼55 MHz for DBT:Ac and DBT:DBN, respectively (see insets in Figure 1). In the first case, the line broadening, compared to before the shift procedure, is unchanged and is attributed to the higher temperature of about 3.5 K at which the experiment is held. Spectral wandering is present in these samples and is related to the fluctuations of the local electric field, due to charge migrations. The energy shift in DBT emission persists even after the pump is turned off for about 24 h, ruling out the hypothesis of temporary heating effects. Furthermore, the frequency increment after each probe scan (single row in the color map), on the order of a few line widths, hints at the possibility of a fine calibration of the effect, which is analyzed in more details in the following sections.

The number of DBT molecules exposed to the laser confocal illumination (beam diameter $d \approx 1 \ \mu$m) is different in the two host−guest systems. On a sample of distributed DBT:Ac NCX (Figure 1b), a single nanocrystal can be isolated within the beam area, which implies that typically only one molecule is resonant within a 500 GHz scan of the probe. However, this cannot exclude the presence of broader molecules on the surface that could be weakly resonant with the intense pump laser. The reported frequency shift is always toward longer wavelengths, in agreement with the characteristic quadratic Stark effect of DBT in Ac.[21] On the other hand, within the highly doped DBN flakes, the confocal volume typically contains several chromophores within a 10 GHz scan of the probe-laser frequency. As reported in Figure 1c, shifts with opposite signs are observed within the sample of DBT:DBN, for which a large linear Stark coefficient has been reported.[22] Importantly, although each individual molecule may sense slightly different local electric fields (see the SI for more information), the fairly homogeneous response of most emitters in this well-defined system indicates that the laser-induced effect acts on all emitters within the diffraction-limited volume. These results jointly corroborate the interpretation of a laser-induced electric field buildup, leading to a Stark effect.

It is worth noticing that, when the pump is switched on, the measurements exhibit a strong background signal, which scales

linearly with power. This light might be due to the presence of several DBT molecules within the illumination volume in the host matrices, weakly excited by the high-power pump laser. We note that such background shows much higher variability in the case of DBT:Ac than for DBT:DBN (Figure 1b,c), as expected, since fewer molecules are involved in the former system. The role of nearby nonresonant DBT molecules in the shifting mechanism is thoroughly discussed further in the manuscript and in the Supporting Information. Notably, the emission purity for single-photon-based applications is not compromised by such background levels (see SI, Figure S3), since the pump power employed for single-photon source operation is much lower than that used to shift the ZPL frequency, yielding a negligible background level.[26] In particular, the statistical analysis of $g^{(2)}(t)$ measurements on 40 DBT:Ac nanocrystals performed in our previous work[27] yields a single-photon purity higher than 97% for 82% of the cases.

In the following, we discuss in detail the shift dependence on pump-burst duration, power, and wavelength.

Characterization of the Light-Induced Frequency Shift. The results on the dynamics of the optical tuning are analyzed in Figure 2, where the frequency shifts of individual molecules in the two host–guest systems are displayed (Figure 2a,b for DBT:Ac and Figure 2c for DBT:DBN). The experimental data represent the ZPL central frequency as a function of the cumulative pump exposure time and are extracted from the temporal map of the probe excitation spectrum *via* Lorentzian fits. As the pictured data suggest, in each observed case the frequency shift slows down for long exposure times, with a characteristic time that typically varies among emitters and is, on average, different in the investigated matrix hosts. In general, such behavior can be fairly well described as a power-law function of time[28] (dashed red lines in the figure are fits to the experimental data):

$$\nu(t) = \nu(0) + \beta(P)(t/t_0)^{\alpha} \tag{1}$$

where ν is the molecule's ZPL central frequency, $\nu(0)$ its initial value, t the cumulative pump-exposure time, $t_0 = 1$ s the time normalization constant, α the power exponent, and the parameter $\beta(P)$ describes the extent of the frequency shift that can be achieved in a given exposure time. The specific dynamic parameters for the molecule's ZPL can vary among the two host matrices and even between different molecules within the same sample. This might be due to local differences in DBT concentration/orientation and to local crystalline impurities.

Interestingly, no clear difference is observed in the induced shifts upon variation of the pump laser wavelength over a range of several nanometers (see also the SI). This suggests that the shift phenomenon can only be partially due to photon absorption by the shifting molecule. Indeed this eventuality is ruled out by tuning the pump laser to the red of the molecule's ZPL, where no excited states exist. Figure 2a shows in yellow dots the results of such an experiment, performed interrupting the pump illumination at regular intervals for about 1 h time. Despite a pump detuning of 10 GHz, a large frequency shift of >20 GHz is observed. Every DBT emitter conversely shows a clear dependence on the pump-laser power. Specifically, when comparing shifts induced in the very same molecule, the parameter β is strictly increasing with the pump laser power and, for short enough illumination times, has a linear dependence. In Figure 2b two frequency shifts operated

on the same molecule, exposed to different values of the pump laser power, are compared. In particular, for the higher power the ZPL is probed during brief interruptions of the pump illumination every few minutes, since a real-time measurement is precluded by the increased background fluorescence. In the inset of Figure 2b, a collection of data is displayed for a molecule in a different nanocrystal, which exhibits considerably larger frequency shifts and enables a characterization for low pump power values. In this case the experimental data represent the overall frequency shifts observed after single illumination bursts of 2 min each with increasing pump power, illustrating the linear behavior of $\beta(P)$ for short illumination time. This result rules out the possibility of the direct two-photon-induced photoionization of the matrix, which would have a quadratic power dependence.

Qualitatively similar trends are reported for DBT:DBN in Figure 2c, where two DBT emitters in the same DBN crystal are simultaneously shifted using a sequence of short, high-power, laser bursts. The burst duration varies between 0.5 and 3 s with a constant laser power of 6 mW. While one of the molecules undergoes photobleaching or large spectral jump during the process, the other accumulates a total shift of 4 GHz in less than 40 s of cumulative excitation. More results on intermolecular differences in the DBT:DBN system are available in the SI.

We note that for the results presented in Figure 2a–c, the modest fluctuations overlapping with the frequency shift in the emission can be related to spectral wandering, which is enhanced at the high power levels reached during pump exposure.

Tuning Molecules into Resonance. The advantages of the all-optical frequency tuning presented here are its spatial resolution and the flexibility of operation. Indeed, the effect is directly activated on the emitting sample with no need for additional nanofabrication steps (*e.g.*, lithography or etching in order to define the electrodes), and, being confined to the confocal beam volume, it enables spatial resolution at the micron level. On the other side, once doped with single-molecule concentration, homogeneously deposited on the substrate *via* drop-casting and desiccation,[27] or even integrated in nanophotonic structures,[15] DBT:Ac nanocrystals allow for spatial isolation of individual molecules, which can thus be selectively tuned by laser focusing. This is shown in Figure 3, where the ZPL peaks of five nearby molecules, each contained in a different nanocrystal (data of different color), are probed at regular time intervals while exposing only one of the molecules to 2 min long laser pulses with increasing power. The corresponding molecule (blue in the figure) undergoes a large shift of about 100 GHz (∼0.20 nm, corresponding to about a fifth of the inhomogeneous broadening and 2000 times the natural line width), whereas the transition frequency of others is not affected. In the inset, a wide-field fluorescence map shows the location of the respective nanocrystals, labeled with the same color code as in the main figure. Their relative distance amounts to approximately 10 μm and is determined by the NCX suspension density before deposition. We note in passing that the limit to the spatial resolution of this approach has not been touched here and is likely determined by the specific charge migration mechanism in the sample.

Finally, we show the scalability of the proposed tuning approach, by shifting independently in a controlled way the ZPL of up to five close-by molecules, which are all brought on resonance within twice their line width. As in the case of the
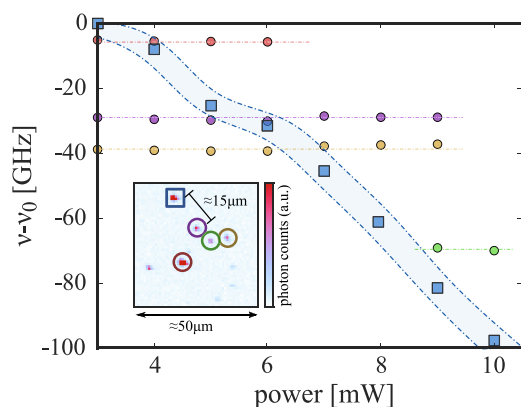
Figure 3. Localized frequency tuning. The central frequency of the ZPL is reported for several molecules as a function of the pump laser power, which only affects one of them (blue squares). The spatial distribution of the doped nanocrystals is given in the inset fluorescence map, revealing that as-close-as-15 μm molecules are completely unaffected by the manipulation.

measurements shown in Figure 3, the emitters are embedded in different nanocrystals. Moreover their emission line widths, shown with the dashed lines in Figure 4, are originally well-separated by 20 GHz. The nanocrystals are addressed by the confocal pump-beam spot one after the other, independently, in order to shift their initial transition frequencies to a common targeted value. The latter, because of the dominant quadratic Stark effect in the Ac-matrix, is necessarily chosen as $\nu_0 \leq \nu_i$, where i labels the molecules' original emission frequencies. Based on previous calibration, the magnitude of the shift is adjusted by controlling the radiation dose (illumination power per exposure time). In general, the time required to shift the emission to a target frequency, which depends on the overall shift width, can be brought down to few minutes by playing on the pump laser power, as described in Figure 2b. This is sufficiently quick to enable successive corrections for possible frequency deviations and hence preserve the target position for the time required to perform an experiment. The final excitation spectra are reported in Figure 4 using solid lines with shaded underlying areas in different colors, demonstrating

fine-matching of five molecules, within about a two-line width range. Total shifts of up to about 20 GHz can be estimated by comparing the final values with the initial ones. In Figure 4b, the relative wide-field fluorescence map is reported, showing the simultaneous excitation of all molecules by means of the probe beam centered at the targeted frequency ν_0. Correspondingly, the bright spots highlight the spatial configuration of the synchronized nanocrystals. We finally observe that similar results have been obtained on different substrates, with nanocrystals deposited either on gold (SI), with a total shift of more than 20 GHz, or on sapphire (Figure 4). In particular, the current residual detuning of about two line widths reported for five molecules and one line width for two molecules only depends on the spectral fluctuations arising during the pump-exposure process. Several mitigation techniques could be suitably implemented in the future to monitor and control the mutual frequency overlap of the emitters' ensemble, including an additional electrical bias to stabilize local charges.

The demonstrated results clearly show together several advantages of the proposed tuning approach: scalability, flexibility in the choice of substrate, high spectral and spatial resolution, and broad tunability range compared to the system's inhomogeneous broadening. We believe such characteristics will be crucial for the coupling of multiple emitters together in linear optical computing or simulation experiments and for the integration of molecules into resonant photonic structures.

Photoionization Model of the Laser-Induced Charge Separation. In this section we propose a possible mechanism for our hypothesis of the laser-induced charge separation through photoionization of DBT molecules. We postulate a cascade photoionization mechanism for the buildup of the local electric field, *via* formation of long-lived charge-separated states. The proposed model is based on the following assumptions:

1. The laser-induced excitation of DBT molecules leads to their photoionization by electron ejection.

2. The process results in long-lived charge-separated states in the matrix. The initially excited DBT molecules may be regenerated to their neutral state.
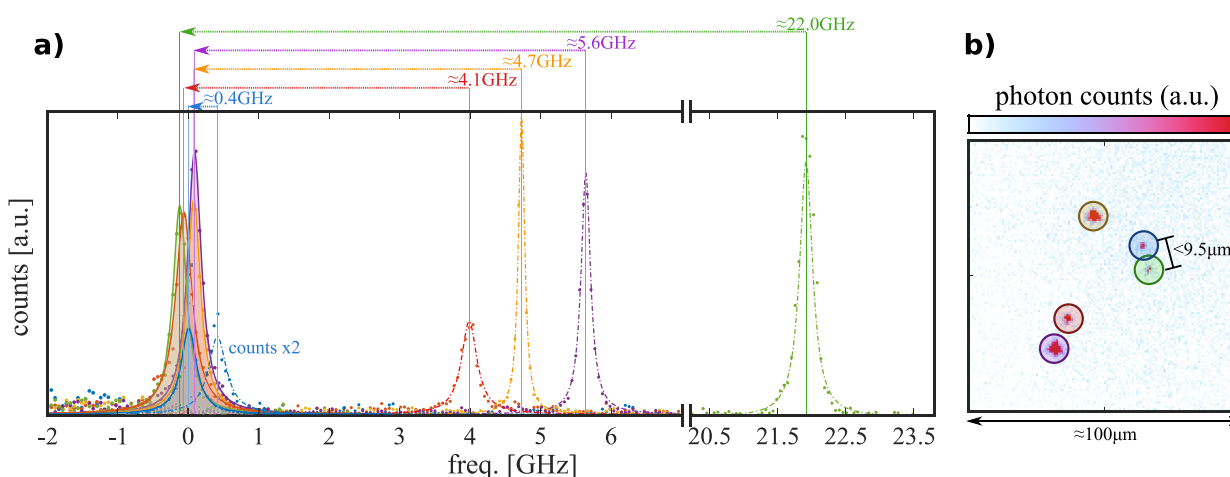

Figure 4. Frequency matching of five distinct molecules can be observed in the excitation spectra displayed in (a) as solid lines with underlying shaded areas. This exceptional condition is the result of a set of individual shifting applied to the original configuration, corresponding to the spectra reported as dashed dotted color lines. (b) Fluorescence map showing the simultaneous excitation of all nanocrystals when the probe is centered around ν_0 and applied in wide-field configuration.

3. The photoionization of DBT results in mobile charge carriers (electrons and holes, with different mobilities) and their transport to larger distances (on the order of tens of nanometers at least).

4. The charge separation and trapping of electrons and holes result in the buildup of a static electric field which shifts DBT's ZPLs through a Stark effect (quadratic for DBT:Ac and linear for DBT:DBN).

The laser-induced charge separation mechanism is outlined in Figure 5. The initial step of the charge generation process is
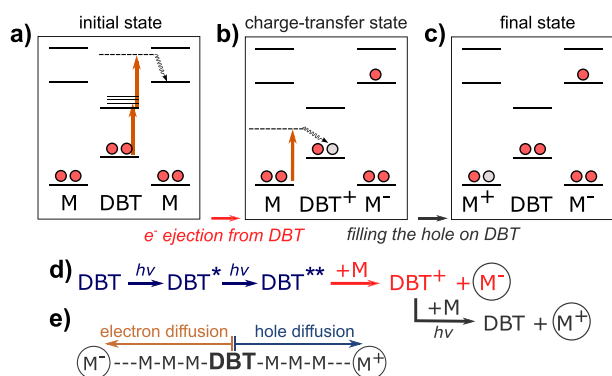

Figure 5. Proposed mechanism of the laser-induced charge generation. (a−c) Electronic energy diagrams describing (a) the initial electronic state and local excitation of DBT (red arrows), followed by electron ejection to the matrix (wavy line), (b) charge-transfer state and filling the hole on DBT, and (c) resulting final state of the system. Transitions induced by a single photon are shown with red arrows, virtual states are indicated by broken lines, and nonradiative CT transitions are indicated by wavy lines. Red and gray circles designate electrons and holes, respectively. M = matrix molecule (DBN or Ac). (d) Photoionization scheme that represents the path sketched in panels (a)−(c). $h\nu$ = energy of a pump-beam photon; excited electronic states are represented with the star symbol. (e) The resulting charge carriers (M^+ and M^-) diffuse further into the charge-separated states under the illumination of the pump beam.

the photoionization of DBT molecules by intense pump light (Figure 5a). This process requires at least two laser photons: a first DBT excitation with one pump photon (1.61 eV for DBT:Ac or 1.96 eV for DBT:DBN) to its first excited electronic state (S1), followed by a further excitation with a second pump photon (red arrows in Figure 5a). Such a highly excited electronic state of DBT can presumably eject an electron to the matrix (M) and give birth to a charge-separated state (DBT^+/M^-). Finally, the hole left on the DBT molecule may be transferred to the matrix through a single-photon excitation (Figure 5b), yielding back a neutral DBT molecule and a matrix cation (M^+) (Figure 5c). Figure 5d summarizes the proposed photoionization cascade. However, while this is one of the most likely mechanisms, we note that other possible channels of light absorption and photoionization are also possible. The presence of dimers or clusters of DBT molecules, for instance, as well as other impurities, can red-shift the absorption spectrum by up to several thousands of cm^{-1}. This can explain the occurrence of the photoionization phenomenon for a broader range of pump frequencies. Notably, we observed that the spectral shifts in both DBT:Ac and DBT:DBN can be induced by using a pump beam at 795 nm, which is outside the inhomogeneous broadening of the

studied systems (200 and 650 cm^{-1} below the ZPL, respectively).

The migration of the induced charge carriers is possibly further activated by the pump beam, leading to charge diffusion and to charge-separated states (M^+ and M^-) far enough from each other so that the recombination probability becomes negligible (see Figure 5e). It is important to realize that, if the initial DBT molecule is regenerated to its neutral state, the process can be repeated many times. In effect, each DBT molecule may give rise to a macroscopic charge distribution in its environment. The resulting charge density buildup shifts ZPLs of DBT probe molecules by the Stark effect.

Our photoionization scheme is inspired by earlier models of photoconductivity in organic solids. The inclusion of larger PAH impurities into an anthracene crystal, such as tetracene, significantly reduces the activation energy for the charge-carrier transport.[29−31] Likewise, the proposed charge separation mechanism is the key to the photorefractive effect in multicomponent photorefractive materials doped with optically active organic molecules.[32]

The suggested model is consistent with the continuous shift of the molecule's ZPL resonance, as well as with its narrow line, which rules out any heating-induced rearrangements. The Stark shift associated with a net field buildup well captures a shift that can have opposite signs for DBT:DBN, while is only toward longer wavelengths for DBT:Ac. Further details on the consistency between the model and the experimental observations are provided in the SI.

Finally, simple quantum chemistry calculations have been performed, which qualitatively support our photoionization model. All three steps presented in Figure 5 are found to be energetically feasible according to time-dependent density functional theory (TDDFT/B3LYP). For the details of the calculations, the reader is referred to the SI. Beyond the first electronic excitation, several higher electronic states of DBT are found above 3.0 eV, suggesting that excitation of DBT with two red photons is likely to happen under experimental conditions of strong illumination. According to the calculations, the following step of electron transfer to the matrix could be phonon-assisted for DBT in Ac, while a direct excitation of the charge-transfer (CT) state may operate as well for the DBT:DBN system. The formation of the CT excitons on the neighboring molecular sites is considered important for the transport properties of photoexcited organic materials.[33] Nevertheless, due to their short lifetimes,[34,35] the CT states cannot explain the buildup of the stable electric field, which persists for long time after the excitation. These states can be rather considered as the precursors for the photoinduced formation of free electrons and holes, which are separated to larger distances by the pump beam. The transport of charges is further supported by the presence of many host molecules in the crystals, which results in the formation of a quasi-band structure of CT-type electronic states (see the SI).[36] Concerning the regeneration of neutral DBT molecules, several CT transitions are found from Ac to DBT^+ within the energy range of our excitation (1.6 eV). Lastly, the further transfer of charge carriers through the matrix to distances larger than several unit cells is assumed to take place through interaction of charged species with red light. Indeed, we find that Ac^+, Ac^-, and DBT^+ can all absorb red photons, which is in line with other theoretical results.[37]

CONCLUSIONS

We have demonstrated optically induced tuning of light emission from single DBT molecules in two different types of molecular crystals that are of interest for molecule-based integrated quantum devices. Tuning by up to 0.2 nm ($\sim$1/5 of the inhomogeneous broadening) has been observed, persisting for a macroscopic time (several hours), which allows the successive manipulation of several independent molecules. Because of the predictability of the frequency shift, we were able to tune five independent molecules on the same ZPL emission wavelength within twice their line width. Such fine control of an emitter's transition frequency, together with the achievable tuning range, might empower the presented technique in any context involving molecular emitters coupled to resonating photonic structures and/or multiple sources emitting at the same wavelength, such as in optical quantum computation, simulation, and communication.

We emphasize the potential applicability of our methodology to a broad range of host/guest molecular systems. Studying light-induced charge dynamics with single-molecule sensitivity could shed light on the microscopic mechanisms behind photoconductivity in organic solids and motivates the exploitation of single molecules in quantum technologies and molecular electronics. Many possibilities to further fine-tune and manipulate optical transitions of molecules can be envisaged in this context. Finally, tuning light emission of many single emitters by using this simple optical approach may become an important step in integrating single emitters into robust quantum protocols based on molecules.

METHODS

Sublimation Growth of DBT:DBN Single Crystals. 2,3-Dibromonaphthalene used in this work was purchased from Ark Pharm Inc. High-quality single crystals of zone-refined DBN doped with dibenzoterrylene molecules were obtained by co-sublimation at $\sim$0.2 bar of argon gas. To prevent perturbations from the convection flow in the sublimation chamber, the sublimator was kept horizontal during growth. The sublimation-grown crystals develop along the (a,b) plane as thin mm-sized plates or flakes, with a typical thickness of a few microns along the c-axis.

Preparation of DBT:Ac Nanocrystals. Nanocrystals (NCs) of anthracene doped with a single-molecule concentration of DBT are grown by injecting 100 μL of a 4:107 mixture of 1 mM DBT−toluene and 5 mM Ac−acetone solutions into 2 mL of sonicating Milli-Q water. After 30 min of sonication, solvents are completely dissolved and DBT:Ac NCs are formed as an aqueous suspension (for more details see ref S1). The nanocrystals are then deposited on the substrate *via* drop-casting of $\sim$10 μL of the suspension followed by desiccation. In particular, the substrates employed in the experiment are simple glass coverslips and coverslips coated with sputtered gold (film thickness of $\sim$200 nm). After the deposition, NCs are protected from sublimation by spin-coating a 200 nm thick layer of poly(vinyl alcohol) (PVA). Solvents Ac and PVA were purchased from Sigma-Aldrich, water was deionized by a Milli-Q Advantage A10 system (resistivity of 18.2 M$\Omega \times$ cm at 25 °C), and DBT was purchased from Mercachem.

Optical Microscopy (DBT:DBN). All single-molecule measurements with DBT:DBN crystals were done at 1.2 K in a home-built liquid-helium bath cryostat. Single crystals of DBT:DBN were optically attached to a glass substrate containing interdigitated gold markers previously deposited by lithography, which served to locate different parts of the single crystal in consecutive experiments. All pump excitation experiments on DBT:DBN were performed on the crystal parts that were in contact with the glass substrate. Single DBT molecules were excited by a tunable continuous-wave Ti:sapphire laser (M Squared) at around 756.7 $\pm$ 0.2 nm. This laser is denoted in

the text as a probe (laser) beam. The frequency range of typically 10 GHz was scanned with 1000 points and 5 ms integration time per point, with a typical power of 0.3 to 0.7 μW focused on the sample. The output of the laser was continuously monitored by an external Fabry−Perrot cavity. The response of this cavity was used to monitor the laser frequency drift in real time and to compensate for a small nonlinearity of the frequency scan. A second, more intense (pump) laser beam was used to induce spectral shifts in DBT:DBN crystals. The laser light was produced by a Coherent ring laser, operated with rhodamine 101 (640) dye and pumped with a 532 nm solid-state laser. The operating wavelength of the pump laser was at around 631 nm, and a typical power focused on the sample was 10 μW to 5 mW. In all experiments the sample was scanned with either only a probe laser (756.7 nm) or simultaneously with both pump (631 nm) and probe lasers focused on the sample. The sample was scanned in a confocal epi-fluorescence arrangement using a scanning mirror (Newport, FSM-300-01). A λ/4 wave plate was used to produce a circularly polarized beam for more efficient excitation of single DBT emitters. The fluorescence light was collected by a cryogenic objective (Microthek, NA = 0.8) and detected by a single-photon counting module (Excelitas SPCM-AQRH-16) with a set of filters (Chroma HQ760LP and Semrock FF02-809/81) in the detection path.

Optical Microscopy (DBT:Ac). The optical characterization of individual DBT molecules in Ac NCs was performed with a home-built scanning fluorescence confocal microscope. All measurements were done at about 3.5 K, with the sample in a closed-cycle helium cryostat (Cryostation by Montana Instruments). The transition line width of individual molecules was measured under confocal resonant excitation, with a CW distributed feedback diode laser (Toptica, LD-0785-0080-DFB-1), named probe in the paper, which is centered at 784.6 nm and can be scanned continuously in frequency over a range of 800 GHz. Frequency shifts of molecules emission were generally induced in off-resonant configuration by using a CW external-cavity diode laser (Toptica, DLX110), named pump in the paper, centered at 767 nm and operated at higher power (also in confocal mode). In particular, the laser frequency can be tuned through fine tilting of the Bragg grating of the diode source, enabling mode-tuning within about $\pm$4 nm around the central value. Laser-induced shifting was also performed by using the probe laser operated at higher power. All laser sources were fiber-coupled and linearly polarized by means of a half-wave plate in the excitation path to allow for optimal coupling to the single molecules' linear dipole. The excitation light was focused onto the sample by a glass-thickness-compensation air objective (Opto-Sigma 50$\times$, NA = 0.67, WD = 10.48 mm) and scanned over the sample by a telecentric system and a dual-axis galvo-mirror. The Stokes-shifted fluorescence was hence separated from the excitation light through a dichroic mirror (Semrock FF776-Di01) and a long-pass filter (Semrock RazorEdge LP02-785RE-25) and detected by either an EMCCD camera (Andor iXon 885, 1004 $\times$ 1002 pixels, pixel size 8 mm $\times$ 8 mm), for measuring fluorescence space-maps and spectral properties, or by a SPAD (SPCM-AQRH-14-TR by Excelitas). A converging lens was inserted in the excitation path, just before the dichroic mirror, to switch between confocal and wide-field illumination. For the antibunching measurement shown in the SI, we employed a Hanbury-Brown and Twiss configuration, based on a fibered beam splitter, two fiber-coupled SPADs (SPCM-800-14-FC by Excelitas), and a time-correlated single-photon counting (TCSPC) card (PicoHarp 300 by PicoQuant). Fiber-coupling of the single-molecule fluorescence was achieved by means of an adjustable fiber-collimator and a free-space telescope for mode-matching.

ASSOCIATED CONTENT

ⓢ Supporting Information

The Supporting Information is available free of charge at https://pubs.acs.org/doi/10.1021/acsnano.0c05620.

Shift dependence of the pump power and independence of the sample substrate; excitation spectrum and antibunching measurement for DBT:Ac; examples of

single-molecule trajectories and power-law fits for DBT:DBN and DBT:naphthalene; quantum chemistry calculations and consistency of the model with experiments (PDF)

AUTHOR INFORMATION

Corresponding Authors

Michel Orrit − *Huygens-Kamerlingh Onnes Laboratory, LION, 2300 RA Leiden, The Netherlands;* orcid.org/0000-0002-3607-3426; Email: orrit@physics.leidenuniv.nl

Costanza Toninelli − *European Laboratory for Non-Linear Spectroscopy (LENS), Sesto F.no 50019, Italy; National Institute of Optics (CNR-INO), 50019 Sesto F.no, Italy;* orcid.org/0000-0002-6843-058X; Email: toninelli@lens.unifi.it

Authors

Maja Colautti − *National Institute of Optics (CNR-INO), 50019 Sesto F.no, Italy; European Laboratory for Non-Linear Spectroscopy (LENS), Sesto F.no 50019, Italy*

Francesco S. Piccioli − *National Institute of Optics (CNR-INO), 50019 Sesto F.no, Italy*

Zoran Ristanović − *Huygens-Kamerlingh Onnes Laboratory, LION, 2300 RA Leiden, The Netherlands*

Pietro Lombardi − *National Institute of Optics (CNR-INO), 50019 Sesto F.no, Italy; European Laboratory for Non-Linear Spectroscopy (LENS), Sesto F.no 50019, Italy*

Amin Moradi − *Huygens-Kamerlingh Onnes Laboratory, LION, 2300 RA Leiden, The Netherlands*

Subhasis Adhikari − *Huygens-Kamerlingh Onnes Laboratory, LION, 2300 RA Leiden, The Netherlands*

Irena Deperasinska − *Institute of Physics, Polish Academy of Sciences, 02-668 Warsaw, Poland*

Boleslaw Kozankiewicz − *Institute of Physics, Polish Academy of Sciences, 02-668 Warsaw, Poland;* orcid.org/0000-0002-2507-2356

Complete contact information is available at:
https://pubs.acs.org/10.1021/acsnano.0c05620

Author Contributions

M.C., F.S.P., and Z.R. are first coauthors. C.T. and M.O. equally contributed to the coordination of this study. M.C., F.S.P., and P.L. performed the experiments on DBT in anthracene. Z.R., A.M., and S.A. performed the experiments on DBT in 2,3-dibromonaphthalene and naphthalene. I.D. performed the quantum chemistry calculations and together with B.K. contributed to the photoionization model. C.T. and M.O. coordinated the research. All authors contributed to the final manuscript.

Notes

The authors declare no competing financial interest.

REFERENCES

(1) Hettich, C.; Schmitt, C.; Zitzmann, J.; Kühn, S.; Gerhardt, I.; Sandoghdar, V. Nanometer Resolution and Coherent Optical Dipole Coupling of Two Individual Molecules. *Science* **2002**, *298*, 385−389.

(2) Pototschnig, M.; Chassagneux, Y.; Hwang, J.; Zumofen, G.; Renn, A.; Sandoghdar, V. Controlling the Phase of a Light Beam with a Single Molecule. *Phys. Rev. Lett.* **2011**, *107*, No. 063001.

(3) Wang, D.; Kelkar, H.; Martin-Cano, D.; Rattenbacher, D.; Shkarin, A.; Utikal, T.; Götzinger, S.; Sandoghdar, V. Turning a Molecule into a Coherent Two-Level Quantum System. *Nat. Phys.* **2019**, *15*, 483−489.

(4) Orrit, M.; Bernard, J. Single Pentacene Molecules Detected by Fluorescence Excitation in a *p*-Terphenyl Crystal. *Phys. Rev. Lett.* **1990**, *65*, 2716−2719.

(5) Basché, T.; Moerner, W. E.; Orrit, M.; Talon, H. Photon Antibunching in the Fluorescence of a Single Dye Molecule Trapped in a Solid. *Phys. Rev. Lett.* **1992**, *69*, 1516−1519.

(6) Lounis, B.; Moerner, W. E. Single Photons on Demand from a Single Molecule at Room Temperature. *Nature* **2000**, *407*, 491−493.

(7) Nicolet, A. A. L.; Bordat, P.; Hofmann, C.; Kol'chenko, M. A.; Kozankiewicz, B.; Brown, R.; Orrit, M. Single Dibenzoterrylene Molecules in an Anthracene Crystal: Main Insertion Sites. *ChemPhysChem* **2007**, *8*, 1929−1936.

(8) Lettow, R.; Rezus, Y. L. A.; Renn, A.; Zumofen, G.; Ikonen, E.; Götzinger, S.; Sandoghdar, V. Quantum Interference of Tunably Indistinguishable Photons from Remote Organic Molecules. *Phys. Rev. Lett.* **2010**, *104*, 123605.

(9) Rezai, M.; Wrachtrup, J.; Gerhardt, I. Coherence Properties of Molecular Single Photons for Quantum Networks. *Phys. Rev. X* **2018**, *8*, No. 031026.

(10) Troiani, F.; Ghirri, A.; Paris, M.; Bonizzoni, C.; Affronte, M. Towards Quantum Sensing with Molecular Spins. *J. Magn. Magn. Mater.* **2019**, *491*, 165534.

(11) Tian, Y.; Navarro, P.; Orrit, M. Single Molecule as a Local Acoustic Detector for Mechanical Oscillators. *Phys. Rev. Lett.* **2014**, *113*, 135505.

(12) Lombardi, P.; Ovvyan, A. P.; Pazzagli, S.; Mazzamuto, G.; Kewes, G.; Neitzke, O.; Gruhler, N.; Benson, O.; Pernice, W. H. P.; Cataliotti, F. S.; Toninelli, C. Photostable Molecules on Chip: Integrated Sources of Nonclassical Light. *ACS Photonics* **2018**, *5*, 126−132.

(13) Türschmann, P.; Rotenberg, N.; Renger, J.; Harder, I.; Lohse, O.; Utikal, T.; Götzinger, S.; Sandoghdar, V. Chip-Based All-Optical Control of Single Molecules Coherently Coupled to a Nanoguide. *Nano Lett.* **2017**, *17*, 4941−4945.

(14) Rattenbacher, D.; Shkarin, A.; Renger, J.; Utikal, T.; Götzinger, S.; Sandoghdar, V. Coherent Coupling of Single Molecules to On-chip Ring Resonators. *New J. Phys.* **2019**, *21*, No. 062002.

(15) Colautti, M.; Lombardi, P.; Trapuzzano, M.; Piccioli, F. S.; Pazzagli, S.; Tiribilli, B.; Nocentini, S.; Cataliotti, F. S.; Wiersma, D. S.; Toninelli, C. A 3D Polymeric Platform for Photonic Quantum Technologies. *Adv. Quantum Technol.* **2020**, *3*, 2000004.

(16) Aumaitre, C.; Morin, J.-F. Polycyclic Aromatic Hydrocarbons as Potential Building Blocks for Organic Solar Cells. *Chem. Rec.* **2019**, *19*, 1142−1154.

(17) Yang, B.; Trebbia, J.-B.; Baby, R.; Tamarat, P.; Lounis, B. Optical Nanoscopy with Excited State Saturation at Liquid Helium Temperatures. *Nat. Photonics* **2015**, *9*, 658−662.

(18) Wild, U. P.; Güttler, F.; Pirotta, M.; Renn, A. Single Molecule Spectroscopy: Stark Effect of Pentacene in p-Terphenyl. *Chem. Phys. Lett.* **1992**, *193*, 451−455.

(19) Orrit, M.; Bernard, J.; Zumbusch, A.; Personov, R. Stark Effect on Single Molecules in a Polymer Matrix. *Chem. Phys. Lett.* **1992**, *196*, 595−600.

(20) Tamarat, P.; Lounis, B.; Bernard, J.; Orrit, M.; Kummer, S.; Kettner, R.; Mais, S.; Basché, T. Pump-Probe Experiments with a Single Molecule: ac-Stark Effect and Nonlinear Optical Response. *Phys. Rev. Lett.* **1995**, *75*, 1514−1517.

(21) Schädler, K.; Ciancico, C.; Pazzagli, S.; Lombardi, P.; Bachtold, A.; Toninelli, C.; Reserbat-Plantey, A.; Koppens, F. H. L. Electrical Control of Lifetime-Limited Quantum Emitters Using 2D Materials. *Nano Lett.* **2019**, *19*, 3789−3795.

(22) Moradi, A.; Ristanović, Z.; Orrit, M.; Deperasińska, I.; Kozankiewicz, B. Matrix-Induced Linear Stark Effect of Single Dibenzoterrylene Molecules in 2,3-Dibromonaphthalene Crystal. *ChemPhysChem* **2019**, *20*, 55−61.

(23) Fiset-Cyr, A.; Dalacu, D.; Haffouz, S.; Poole, P. J.; Lapointe, J.; Aers, G. C.; Williams, R. L. *In-Situ* Tuning of Individual Position-Controlled Nanowire Quantum Dots *via* Laser-Induced Intermixing. *Appl. Phys. Lett.* **2018**, *113*, No. 053105.

(24) Takahashi, M.; Syafawati Humam, N.; Tsumori, N.; Saiki, T.; Regreny, P.; Gendry, M. Local Control of Emission Energy of Semiconductor Quantum Dots Using Volume Expansion of a Phase-Change Material. *Appl. Phys. Lett.* **2013**, *102*, No. 093120.

(25) Grim, J. Q.; Bracker, A. S.; Zalalutdinov, M.; Carter, S. G.; Kozen, A. C.; Kim, M.; Kim, C. S.; Mlack, J. T.; Yakes, M.; Lee, B.; Gammon, D. Scalable in *Operando* Strain Tuning in Nanophotonic Waveguides Enabling Three-Quantum-Dot Superradiance. *Nat. Mater.* **2019**, *18*, 963−969.

(26) Lombardi, P.; Trapuzzano, M.; Colautti, M.; Margheri, G.; Degiovanni, I. P.; López, M.; Kück, S.; Toninelli, C. A Molecule-Based Single-Photon Source Applied in Quantum Radiometry. *Adv. Quantum Technol.* **2020**, *3*, 1900083.

(27) Pazzagli, S.; Lombardi, P.; Martella, D.; Colautti, M.; Tiribilli, B.; Cataliotti, F. S.; Toninelli, C. Self-Assembled Nanocrystals of Polycyclic Aromatic Hydrocarbons Show Photostable Single-Photon Emission. *ACS Nano* **2018**, *12*, 4295−4303.

(28) Nicolet, A. A. L.; Kol'chenko, M. A.; Hofmann, C.; Kozankiewicz, B.; Orrit, M. Nanoscale Probing of Charge Transport in an Organic Field-Effect Transistor at Cryogenic Temperatures. *Phys. Chem. Chem. Phys.* **2013**, *15*, 4415−4421.

(29) Silinsh, E. A. *Organic Molecular Crystals: Their Electronic States*, 1st ed.; Springer-Verlag: Berlin, Heidelberg, 1980.

(30) Karl, N. In *Festkörperprobleme XIV*; Queisser, H. J., Ed.; Springer: Berlin, Heidelberg, 1974; pp 261−290.

(31) Hoesterey, D.; Letson, G. The Trapping of Photocarriers in Anthracene by Anthraquinone, Anthrone and Naphtacene. *J. Phys. Chem. Solids* **1963**, *24*, 1609−1615.

(32) Moerner, W. E.; Silence, S. M. Polymeric Photorefractive Materials. *Chem. Rev.* **1994**, *94*, 127−155.

(33) Stadtmüller, B.; Emmerich, S.; Jungkenn, D.; Haag, N.; Rollinger, M.; Eich, S.; Maniraj, M.; Aeschlimann, M.; Cinchetti, M.; Mathias, S. Strong Modification of the Transport Level Alignment in Organic Materials after Optical Excitation. *Nat. Commun.* **2019**, *10*, 1470.

(34) Causa', M.; Ramirez, I.; Martinez Hardigree, J. F.; Riede, M.; Banerji, N. Femtosecond Dynamics of Photoexcited C60 Films. *J. Phys. Chem. Lett.* **2018**, *9*, 1885−1892.

(35) Hahn, T.; Tscheuschner, S.; Saller, C.; Strohriegl, P.; Boregowda, P.; Mukhopadhyay, T.; Patil, S.; Neher, D.; Bässler, H.; Köhler, A. Role of Intrinsic Photogeneration in Single Layer and Bilayer Solar Cells with C60 and PCBM. *J. Phys. Chem. C* **2016**, *120*, 25083−25091.

(36) Schwoerer, M.; Wolf, H. C. *Organic Molecular Solids*, 1st ed.; Wiley-VCH: Weinheim, 2008.

(37) Malloci, G.; Joblin, C.; Mulas, G. On-line Database of the Spectral Properties of Polycyclic Aromatic Hydrocarbons. *Chem. Phys.* **2007**, *332*, 353−359.